Linking grassland dynamics to snowmelt timing in the Western Pyrenees

Pablo Domínguez-Aguilar[1], Jesús Revuelto[1], Simon Gascoin[2], Juan I. López-Moreno[1]

[1]Pyrenean Institute of Ecology, CSIC, Zaragoza, 50059, Spain

5 [2]CESBIO, CNRS/CNES/IRD/INRAE, Université de Toulouse, Toulouse, France

Correspondence to: Pablo Domínguez-Aguilar (paguilar@ipe.csic.es)

Abstract. It is now well established that climate change modifies the snow cover regime in European mountains. However, the impact of snow cover changes on alpine ecosystems is not well understood. In this study, we assess how snowmelt timing affects alpine grassland growth (onset and evolution) in the western Spanish Pyrenees using eight years (2018–2025) of

10 Sentinel-2 imagery at 10 m resolution. We combined satellite-derived snow melt-out dates (SMOD) with NDVI time series, meteorological data, and fractional snow-covered area (fSCA) to evaluate the temporal and spatial relationships between snowmelt timing and vegetation greening. Our results confirm that snowmelt consistently influences the onset of greening and regulates the timing of peak NDVI (annual maximum). However, short-term variations in melt-out timing had limited influence on the intensity of peak NDVI, which was more strongly linked to post-melt meteorological conditions. The spatial pattern of

15 peak NDVI remained stable across years despite variable melt timing. Our observations suggest that site-specific characteristics—such as soil properties, microclimate, and vegetation composition—that can be linked to the long-term legacy of snow presence can exert a stronger influence on productivity than year-to-year snowmelt dynamics.

1 Introduction

20 Alpine grasslands play an important ecological role in mountain regions by providing essential services, such as carbon storage, soil protection, nutrient cycling, forage provision and water retention (Mascetti et al., 2023; Qian et al., 2023). Their functioning is strongly influenced by seasonal snow cover, which regulates soil temperature, moisture and nutrient availability (Körner, 2021). In particular, the timing of snow disappearance—the snow melt-out date (SMOD)—is a fundamental variable shaping vegetation dynamics (Jonas et al., 2008; Möhl et al., 2022). Earlier or later melt-out affects both the onset and pace of

25 green-up, as well as the total period available for plant growth (Vitasse et al., 2017; Xie et al., 2020). However, while phenological shifts following melt-out are generally consistent, the consequences on productivity are more variable across regions and vegetation types (Choler, 2015; Heim et al., 2022; Slatyer et al., 2022). In some alpine grasslands, earlier melt-out leads to higher productivity due to an extended growing season (Asam et al., 2018; Choler, 2015), whereas in others it can lead to increased drought stress, reducing biomass accumulation later in summer (Möhl et al., 2023). These contrasting

30 responses are due to the influence of other climatic variables during the growing season. Moreover, species exhibit contrasting phenological strategies that determine their sensitivity to melt-out timing—some initiate growth immediately after snow disappearance, while others respond to accumulated heat or photoperiod thresholds (Baptist et al., 2010; Vorkauf et al., 2021a). As a result, the relationship between SMOD, phenology, and productivity is not uniform, and regional studies are essential to clarify how these processes operate under local climatic and ecological conditions.

35 European mountain ranges are warming more rapidly than the global land surface (Copernicus Climate Change Service (C3S), 2024). Previous studies reported a significant decline in snowpack since the 1950s—both depth and duration—consistent with climatic trends of warming (López-Moreno et al., 2020; Vorkauf et al., 2021b). Barrou Dumont et al. (Barrou Dumont et al., 2025) found that the SMOD occurs earlier at a rate of approximately 5 d decade^{-1} over the period 1986-2024 in the French Alps and the Pyrenees. Bayle et al. (Bayle et al., 2025) found a similar trend over the entire Alpine range (1984-2022). Climate

40 models projections indicate that the atmospheric warming will continue during the 21st century accompanied by a shift in precipitation toward drier summers and more humid winters with a decreasing fraction of precipitation falling as snow (Kotlarski et al., 2023). As a result, a continued reduction of the snow cover duration is expected, further altering the hydrological and ecological dynamics of these environments (Beniston et al., 2018; Dumont et al., 2025). Understanding how SMOD influences alpine grassland growth under current conditions is therefore crucial for anticipating ecological responses

45 to future snowpack changes.

Satellite remote sensing provides a consistent and cost-effective way to monitor snow and vegetation dynamics across broad spatial and temporal scales. However, spatial resolution plays a critical role in capturing ecological variability. While coarse-resolution sensors such as MODIS or AVHRR provide long time series suitable for large-scale analyses, they often smooth out fine-scale heterogeneity of the snow and vegetation patterns that can be captured with higher-resolution imagery from

50 Landsat or Sentinel-2 (Dedieu et al., 2016; Gascoin et al., 2019).

This study focuses on a mountain grassland area in the Pyrenees. In this region, a two-year unmanned aerial vehicle (UAV) imagery-based study in a small subalpine basin helped analyse how the SMOD timing influenced the NDVI evolution of the area, revealing that intermediate melt-out timing—around late April and early May—was associated with the highest NDVI values (Revuelto et al., 2022). On the other hand, Alonso-González et al. (2024) conducted a long-term (1981–2014) study covering the entire Pyrenean range using coarse-resolution (1.1 km) NDVI data from the AVHRR-NOAA mission, combined with statistical modelling. They identified SMOD as the primary driver of interannual fluctuations in peak NDVI (maximum annual value), reinforcing the significance of snow-vegetation coupling at broad spatial and temporal scales.

Building on this previous research, the present study bridges the gap between short-term, fine-scale analyses and long-term, coarse-scale assessments by leveraging eight years (2018–2025) of snow cover and vegetation data at 10 m resolution from Sentinel-2 satellite mission. This dataset has a spatial resolution that is sufficient to capture within-landscape variability and a temporal coverage that is long enough to evaluate interannual variability. Specifically, we test the hypothesis that interannual variability in SMOD significantly affects the magnitude of peak NDVI across a 77 km² grassland area in the Western Pyrenees.

2. Study area

The Pyrenees form a major orographic barrier separating the Iberian Peninsula from the rest of the European continent. Their main axis extends west to east for over 400 km, from the Atlantic Ocean to the Mediterranean Sea, reaching a maximum elevation of 3,404 m a.s.l. at Aneto Peak. This configuration results in marked climatic asymmetries: northern slopes receive higher precipitation due to the interception of humid Atlantic air masses, while southern slopes experience a drier climate. Additionally, a west-to-east gradient exists, with western sectors influenced more heavily by Atlantic conditions and eastern sectors showing increasing Mediterranean influence (López-Moreno et al., 2020). Above 2000 m a.s.l., the snowpack tends to last from December to April (Alonso-González et al., 2020).

Figure 1 shows the study area, which is located in the Western Spanish Pyrenees and spans approximately 77 km². It comprises the headwaters of two river basins—the Aragón and Gállego rivers. It is a topographically heterogeneous area, with elevations ranging from 1500 m a.s.l. at valley bottoms to over 2800 m a.s.l. at the peaks in the cirque surrounding Ip Lake, in the south-western quadrant. In this zone, steep rock faces and scree slopes dominate, resulting in sparse vegetation cover. On the other hand, the remaining quadrants have gentler slopes where grasslands are the dominant vegetation type, although near-treeline forest communities can be found at the lower elevations. Thus, to exclude forested areas and unvegetated rocky peaks, the analysis was restricted to the 1,700–2,600 m a.s.l. elevation band. These grassland areas are seasonally grazed by livestock—primarily cattle, sheep and horses—under extensive farming systems during the warm season.

Embedded within the broader study area is the Izas experimental catchment, a small (~ 0.5 km², ~ 0.65% of the whole study area) subalpine basin located between 2,000 and 2,300 m a.s.l., predominantly facing east. Its vegetation composition and snowpack characteristics are representative of subalpine environments across the central Spanish Pyrenees, making it a useful reference for the surrounding landscape (Revuelto et al., 2017). The experimental catchment is also the site of the UAV-based

study by Revuelto et al. (2022), and in the present work, we make use of data from the automatic weather station (AWS) and time-lapse camera installed there to support snow cover analysis (Revuelto et al., 2016).
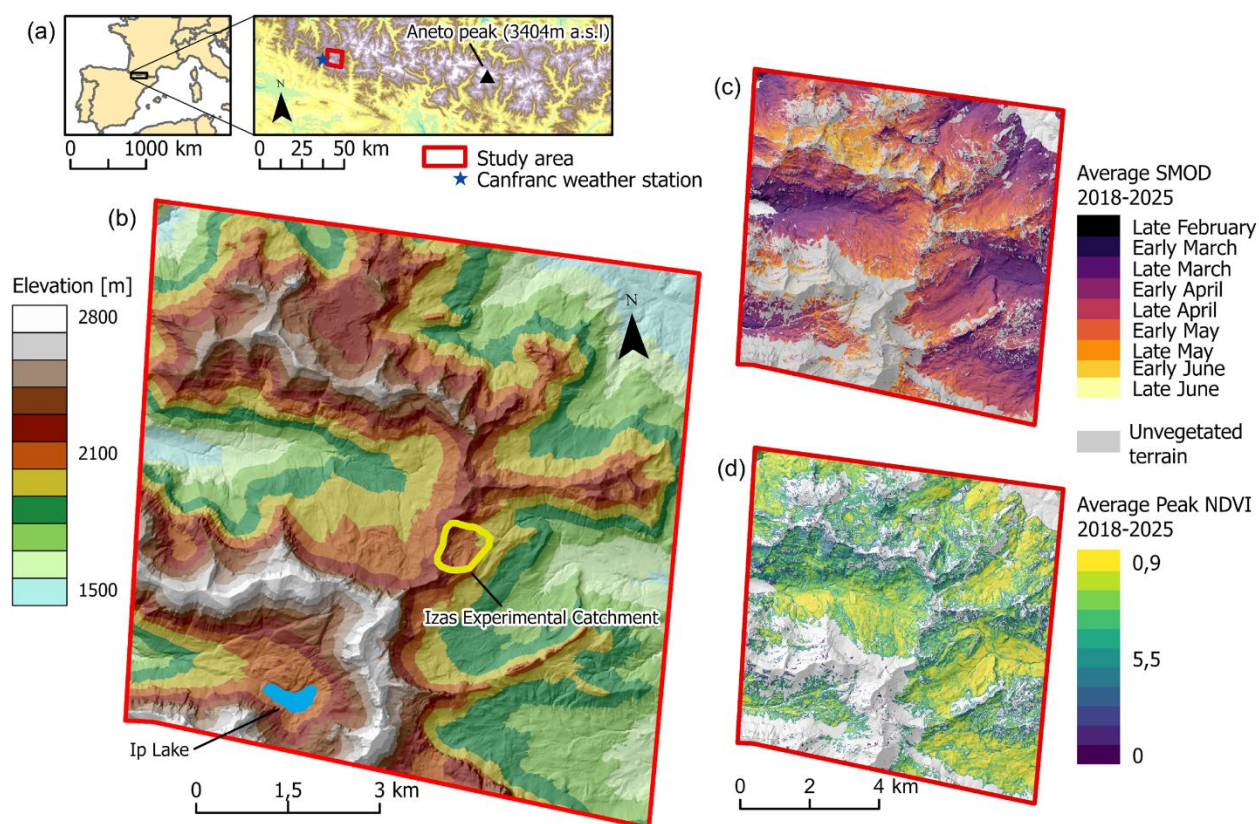
85

Figure 1. Study area summary, including location in the western Spanish Pyrenees (a) and key features (b) (DEMs were obtained from the Spanish National Geographic Institute, IGN). 2018-2025 averages of SMOD (c) and peak NDVI (d) are shown on the right.

3. Methods

90   This study leverages Sentinel-2 L2A imagery from 2018 to 2025. Each acquisition, available with a five-day frequency, consists of atmospherically corrected spectral bands that represent bottom-of-atmosphere (surface) reflectance. These images were processed in the *Google Earth Engine* platform (GEE) to retrieve NDVI and binary snow presence (bSP) maps, and the data analysis was performed with *R* software. Most bands relevant to this study—green (G), blue (B), red (R), and near infrared (NIR)—have a 10 m × 10 m spatial resolution, while Band 11 (short-wave infrared, SWIR) was originally acquired at 20 m

95   × 20 m and resampled using nearest-neighbour interpolation to match the others (Dong et al., 2020; Mullerova & Williams, 2019).

4

3.1. SMOD calculation

bSP maps were generated for every five-day acquisition from February 1 to September 30 of each year. To reduce noise from cloud obscuration, a cloud mask was applied to each image using the *Sentinel 2 Cloud Probability* dataset and *s2cloudless*
100 methodology (Zupanc, 2017). This mask was chosen for its recognized strong performance in snowy scenes compared to similar products—despite its inability to detect cloud shadows (Gao et al., 2024; Skakun et al., 2022), which was accordingly accounted for in later processing steps. After masking clouds out, bSP maps were computed following Gascoin et al. (2019). Snow presence was derived by applying thresholds to the normalized difference snow index (NDSI) and the R band—0.4 for NDSI and 0.2 for the R band. The NDSI was calculated using the formula presented in Table 1. Pixels exceeding both
105 thresholds were classified as snow-covered, while the remaining unmasked pixels were considered snow-free.

Table 1. Applied spectral indices

Spectral index	Formula	Described in
NDSI (normalized difference snow index)	(G - SWIR) / (G + SWIR)	Hall et al. (1995)
NDVI (normalized difference vegetation index)	(NIR - R) / (NIR + R)	Fontana et al. (2008)
NDWI (normalized difference water index)	(G – NIR) / (G + NIR)	Du et al. (2016)
BSI (bare soil index)	(SWIR + R - NIR - B) / (SWIR + R + NIR + B)	Mzid et al. (2021)

To enable time series analysis, these maps were organized into annual sequences, creating eight separate time series stacks. Within each stack, every pixel's snow status was tracked throughout the season, forming a binary temporal profile (snow = 1,
110 snow-free = 0, cloud/missing = no-data). A custom algorithm was developed to identify the timing of melt-out pixel-wise. A melt-out event was defined as the transition from at least 15 consecutive days of snow cover to at least 15 consecutive snow-free days. No-data gaps longer than 10 days caused the sequence to be discarded. The last observed day of snow presence before the onset of the sustained snow-free period was recorded as the SMOD. In cases with multiple qualifying transitions, the earliest melt-out date was retained. If a full transition period was not found, we used partial sequences (≥ 7 snow and ≥ 7
115 snow-free days) to estimate melt-out. When not even such incomplete sequences could be found, SMOD was left undefined for that pixel.

The resulting SMOD values were recorded as day-of-year (DOY) integers, creating a spatial map of melt-out days for every year. These DOY values were subsequently binned into discrete half-month periods. This step assigned each SMOD value to one of 24 intervals, ranging from early January to late December, based on its calendar date. This half-month classification
120 allowed for consistent aggregation (and noise reduction) of snow disappearance timing across years, supporting both quantitative comparison and visual interpretation of spatial melt-out patterns, ensuring sufficient data on each 15-day period—considering the five-day Sentinel acquisition frequency and the impact of cloud obscuration.

3.2. Seasonal and peak NDVI extraction

The same set of Sentinel-2 images was also used to derive NDVI (Table 1) time series for vegetation assessment. NDVI is a
widely used indicator of grassland productivity, reliably tracking field-based measures of growth and biomass while remaining
largely unaffected by topography in mountain terrain (Chen et al., 2020; Choler, 2015). An additional filtering step was applied
to retain only those images with cloud obscuration in the study area below 10% as valid acquisitions. This aimed to reduce the
impact of cloud mask inaccuracies, which can alter NDVI values especially near the edges of clouds or within cloud shadows.
Additional static masks were applied in addition to exclude bare ground and water surfaces. These masks were derived from
a single 100% clear-sky summer image using the bare soil index (BSI) and the normalized difference water index (NDWI)
(Table 1). Pixels classified as bare soil—$BSI \geq 0$ (Mzid et al., 2021)—or water—$NDWI > 0.2$ (Du et al., 2016)—were excluded
from the NDVI analysis (Fig. 1c). Pixel-wise NDVI observations were grouped based on the melt-out period as defined by the
SMOD maps. This allowed the reconstruction of NDVI trajectories classified by their SMOD and analysis of the growth rate
during the green-up phase. This was calculated as the slope of each NDVI curve from the start up to 90% of maximum NDVI,
to exclude the flattening phase occurring before the maximum is reached.

From each annual collection, the map with the highest mean NDVI was selected as the peak NDVI. Pearson's correlation was
computed for all pairs of peak NDVI maps to obtain an assessment on the variability of the NDVI distribution when, in average,
it was at its annual maximum. An "Average peak NDVI" map was created by computing the pixel-wise mean of the eight
annual peak NDVI maps. SMOD maps were treated likewise, computing Pearson's correlation for all pairs as well as
generating an "Average SMOD" map.

3.3. Statistical and climatic analysis

To assess the temporal stability of spatial patterns in peak NDVI and SMOD across the 2018–2025 period, pixel-wise Pearson's
correlation was conducted between all pairs of annual maps for each variable separately. The average of all Pearson's r
coefficients was then calculated as a measurement of peak NDVI and SMOD spatial similarity throughout the period of study.
Linear regression was applied to study the influence of snowmelt timing on a) peak NDVI intensity, and b) peak NDVI timing.
A continuous range of fractional snow-covered area (fSCA) thresholds—from 0.01 to 1 in 0.01 steps—was defined to
characterize snowmelt timing. For each threshold and year, the earliest day on which fSCA dropped below the specified level
was extracted, resulting in a threshold-specific series of melt dates across years. Two datasets were used for this: the Sentinel-
derived bSP maps, corresponding to the whole study area; and a local, high temporal resolution fSCA series of the Izas
experimental catchment.

The Sentinel-based fSCA series was created by clipping each annual bSP series to its corresponding peak NDVI map and
calculating a simple ratio between snow pixels and total pixels in each map. The Izas fSCA series was generated with daily
images from the Campbell CC640 digital camera installed there in September 2011 following the methodology described in

Revuelto et al. (2016). fSCA at 1 m spatial resolution was derived from each available date creating annual time series for the
155 2018-2023 period. 2024 and 2025 series were not available due to a camera malfunction.

Once the threshold analysis was performed, linear models were computed at each SCA threshold level for both peak NDVI intensity and timing using both datasets, allowing the assessment of potential synchrony and the link between vegetation responses at different scales. The p-value was used to evaluate statistical significance and the coefficient of determination (R^2) to evaluate model fit.

160 Lastly, precipitation and temperature data were used to characterize the after-snowmelt periods and observe their potential link with yearly NDVI evolution. Daily precipitation data were obtained from the Canfranc Station (Spanish National Weather Service - AEMET) right outside the western border of the study area (Fig. 1), and aggregated into half month periods. Temperature data were downloaded from the AWS in the experimental catchment (Revuelto et al., 2017) and smoothed with a seven-day moving mean.

165 ## 4. Results

4.1. Seasonal NDVI trajectories

The 2018-2025 average of mean annual NDVI trajectories for each SMOD period is shown in Figure 2 (a). The vegetation growth starts immediately after the snow cover disappearance. The maximum NDVI for each SMOD period changed throughout the season: maximum NDVI reached ~ 0.67 for the earliest melt-out period, increased to its highest value of ~ 0.69
170 for early March, and progressively declined to a minimum of ~ 0.53 for late June melt-out. While earlier melt-out dates led to earlier NDVI peaks, the temporal spread of SMOD (4.5 months) was substantially broader than the range of dates of maximum NDVI (2.5 months). This led to reduced green-up times, ranging from 3.5 months in the earliest melting sites—late February— to 1.5 in the latest melting ones—late June, as well as increasing NDVI growing rates. As shown in Fig. 2 (b), the slope during green-up increased consistently from the earliest SMOD periods to the latest ones, with daily NDVI increments being almost
175 four times larger for late June melting dates than late February ones.
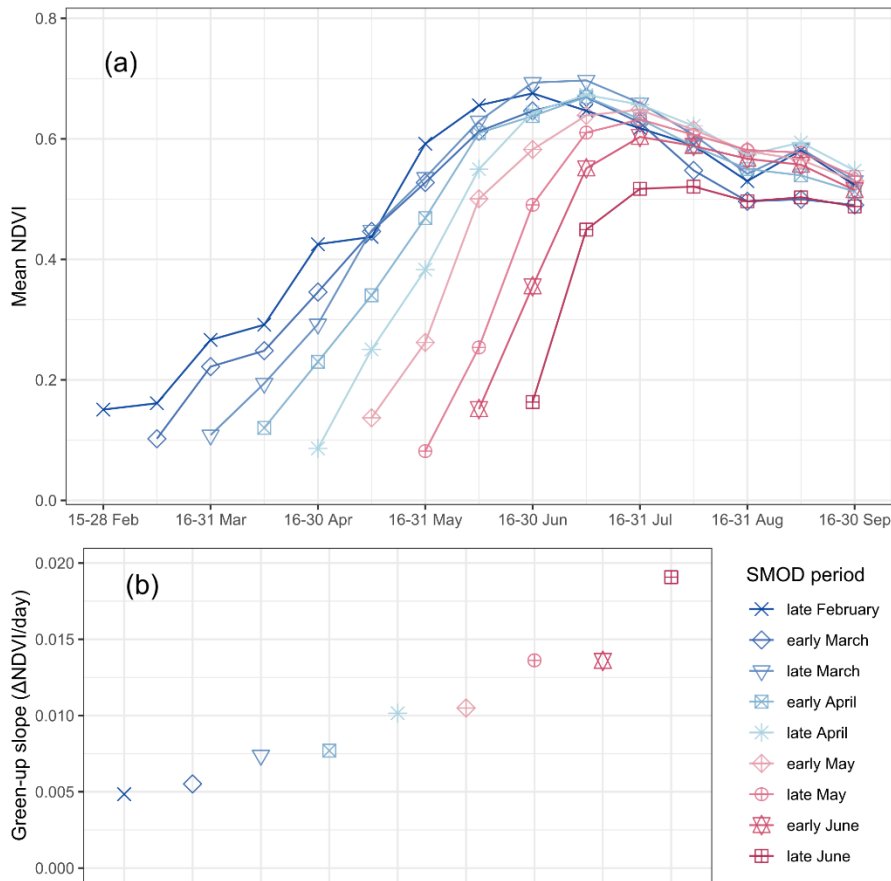
Figure 2. (a) Annual evolution of mean NDVI in each SMOD period zone (Average of the 2018-2025 period). (b) Slope of NDVI curves during growing phase.

4.2. Influence of SMOD on peak NDVI

180   Timing and intensity of peak NDVI during the study period are summarised in Table 2. Peak NDVI consistently occurred in July, although a maximum difference of 21 days was found between the earliest occurrence—2023—and the latest—2018. An average of 28 valid acquisitions were available each year, ignoring the outlier of 2019—most of those additional acquisitions were collected during February and March, at very early stages of vegetation growth.

Table 2. Annual NDVI series summary

	2018	**2019**	**2020**	**2021**	**2022**	**2023**	**2024**	**2025**
Date of peak NDVI	23/07	20/07	07/07	17/07	07/07	02/07	16/07	08/07
Mean peak NDVI	0.69	0.63	0.69	0.69	0.67	0.71	0.66	0.68
Valid acquisitions	26	49	34	26	20	29	31	28

185

The analysis of the linear model fits is presented on Figure 3. Regarding peak NDVI intensity, no significant relationship ($p < 0.05$) was found at any crossing threshold for either of the fSCA series, although a maximum R^2 of 0.53 was obtained at fSCA = 0.03 for the Izas series. However, the models for the timing of peak NDVI reported statistical significance below fSCA = 0.27 for the Sentinel series and fSCA = 0.54 for the Izas series, and showed a stronger link between variables as snowmelt progressed. The maximum fit was obtained at fSCA = 0.03 for the Sentinel series (R^2 = 0.81) and at fSCA = 0.09 for the Izas one (R^2 = 0.83).
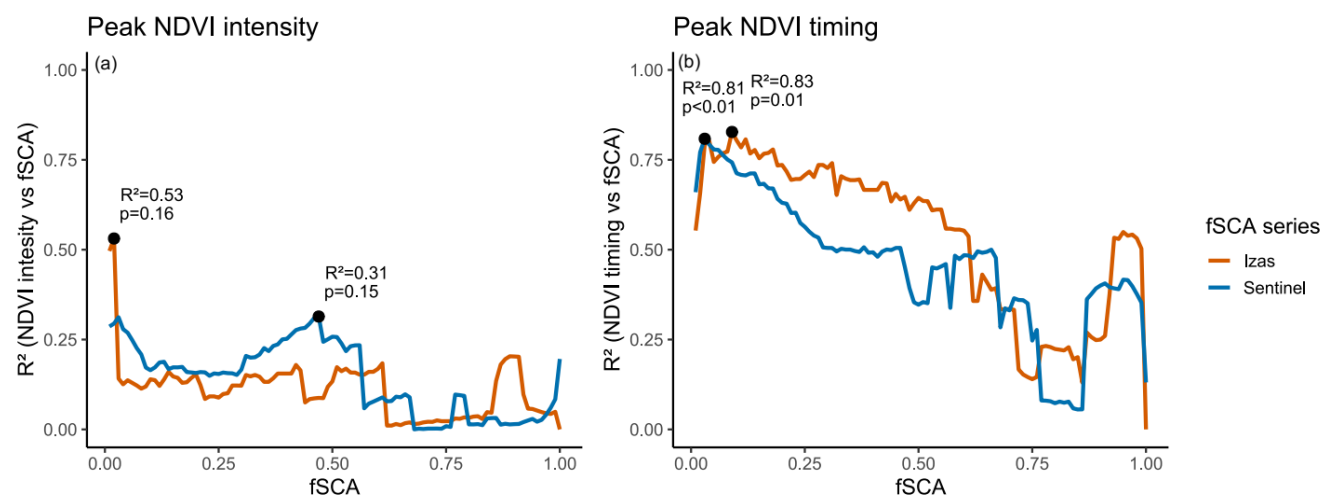

Figure 3. Evolution at each fSCA level of linear model fits between timing of snowmelt and (a) peak NDVI intensity and (b) timing of peak NDVI. Colour-coded for the source of fSCA series.

4.3. Meteorological factors and spatial patterns

Figure 4 focuses on post-snowmelt meteorological conditions and their influence on peak NDVI intensity in three distinct years—2018 presenting the longest-lasting snowpack, 2019 the lowest peak NDVI and 2023 both the shortest-lasting snowpack and highest peak NDVI. In 2019, despite abundant precipitation in April and May, the summer months were dry, and June exhibited both high maximum and low minimum temperatures. In contrast, 2023 experienced a drier spring which was followed by abundant June precipitation and milder temperature extremes. The long-lasting snowpack in 2018 was the result of intense winter precipitation and markedly lower early-spring temperatures. However, from April onwards, both minimum and maximum temperatures returned to a similar range to the other years. Precipitation values in this period also were similar to 2019 and 2023. Early June 2018 was remarkably wet, but the upcoming summer days were the driest of the three years.
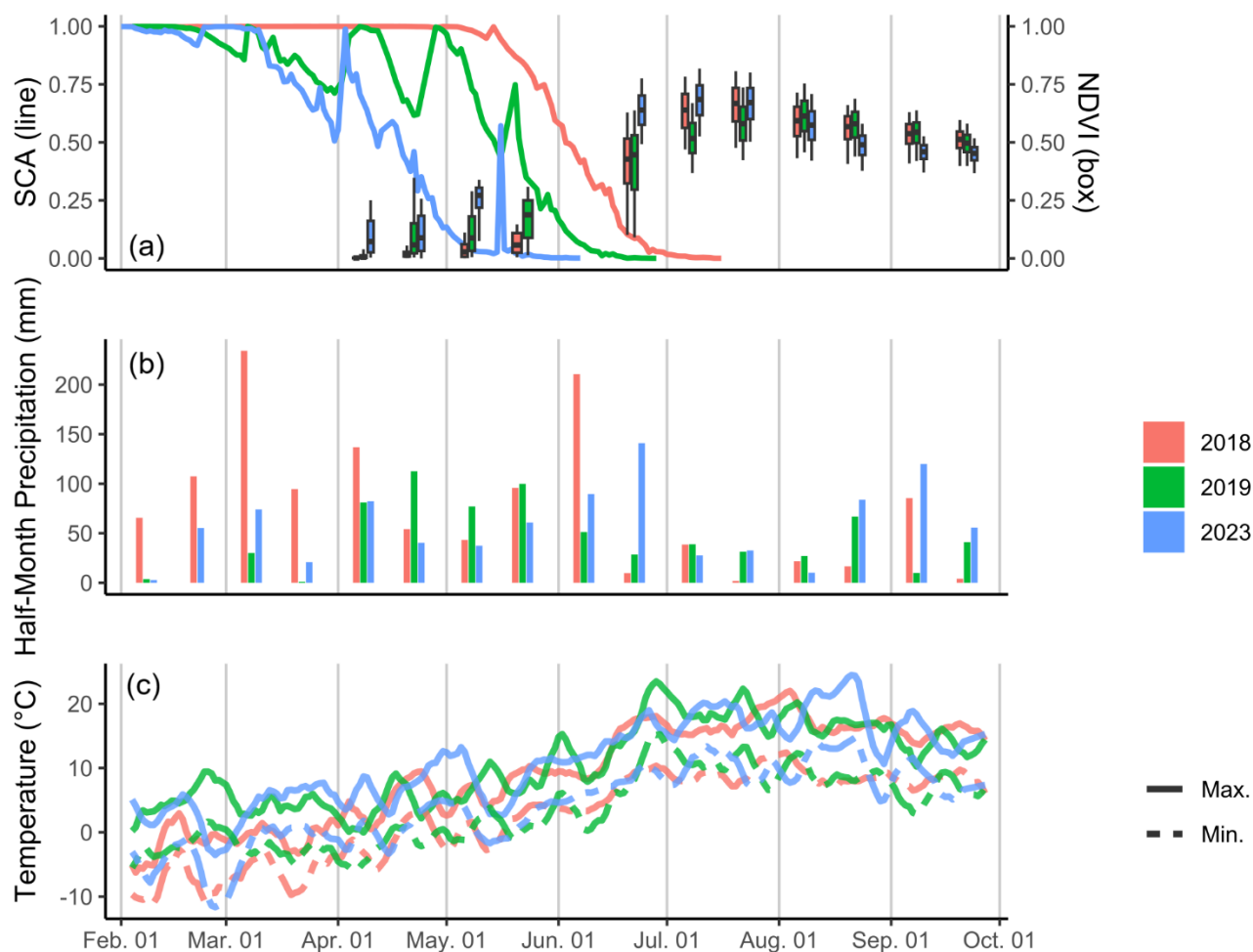
Figure 4. (a) Temporal evolution of fSCA and NDVI. (b) Precipitation from the Canfranc AEMET station, aggregated in 15-day intervals. (c) Maximum and minimum temperatures from the Izas experimental catchment AWS, smoothed by 7-day moving mean.

Figure 5 assesses the relation between the distribution of peak NDVI and SMOD across the years. The focus is on 2019 and 2023—the years with the lowest and highest mean peak NDVI, respectively—and the average peak NDVI and SMOD over the study period. In 2019, median NDVI above 0.75 was not reached in any area, while in 2023, areas melting in March and April reached or exceeded this value. The eight-year average shows the highest NDVI values for melting periods spanning late March to early June, with the highest mean value found in late April. The spatial extent of each melt-out period also varied: early May dominated in 2019 (~ 2500 ha), while 2023 featured an earlier extensive melt in early March (~ 1600 ha). The 2018–2025 average fell between these extremes, with April melt-out periods covering over 2600 ha.
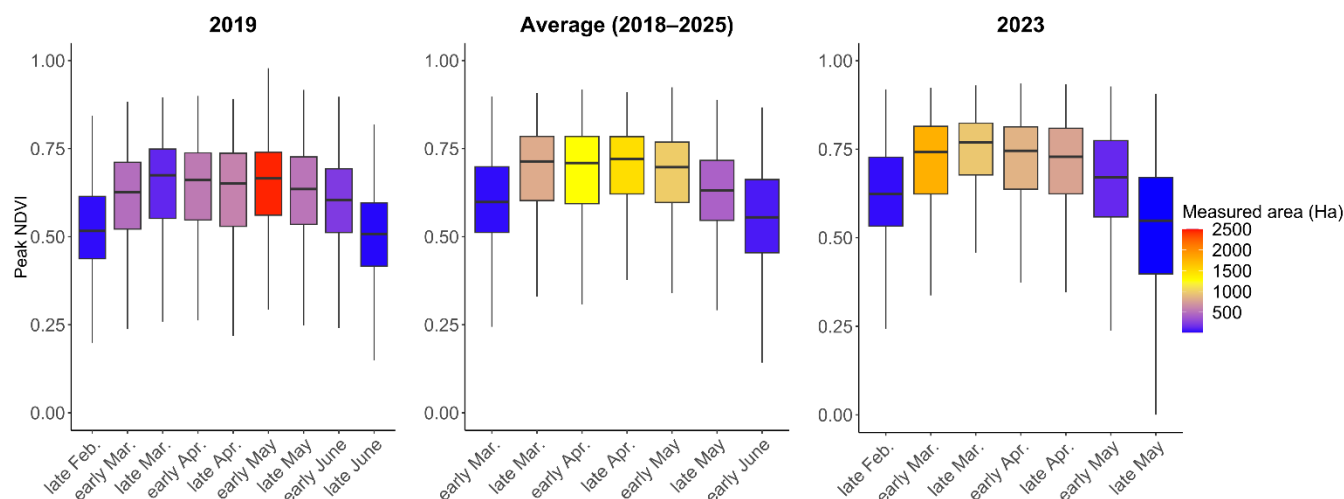
205

210

Figure 5. Distribution of values from the annual peak NDVI map in their corresponding SMOD period, colour-coded for covered area.

Despite these differences in snowmelt timing and extent, the spatial distribution of peak NDVI remained remarkably stable throughout the period of study. Pixel-wise NDVI values were highly correlated across all years (mean Pearson's r = 0.94). Even the correlation of the pair of most extreme peak NDVI years (2019 and 2023) remained strong (Pearson's r = 0.91). By contrast, SMOD maps exhibited greater interannual variability (mean r = 0.77; r = 0.61 between 2019 and 2023), indicating that snowmelt spatial patterns fluctuate more than those of maximum vegetation greening.

5. Discussion

This study aimed to clarify the influence that the timing of snowmelt (SMOD) has on grassland vegetation, both in terms of phenology and productivity. Our results indicate that greening consistently tracks snow disappearance (Figs. 2 and 4), as reported in previous research (Slatyer et al., 2022; Vitasse et al., 2017; Xie et al., 2020). The temporal frequency of Sentinel imagery did not allow for an accurate analysis on whether vegetation growth starts immediately after snow disappearance, but our results suggest a tight temporal coupling. Moreover, the influence of SMOD on the green-up phase duration can be observed in the fact that the NDVI slope during the early growing stage is progressively steeper when SMOD is later. Biological constraints related to photoperiod or accumulated heat could be the main factor explaining these differences (Choler et al., 2024; Tomaszewska et al., 2020). The temporal link between snowmelt and phenology extends until the end of the growing season, when peak productivity is reached (Fig. 3b). The robustness of the linear models based on fSCA at different spatial scales and resolutions reinforces the importance of snowmelt dynamics on grassland phenology.

However, peak annual productivity seems to be independent from snowmelt dynamics. We demonstrated the null linear relationship between timing of increasing levels of snowmelt and the intensity of peak NDVI (Fig. 3a). Additionally, the SMOD period associated with the highest NDVI values in each peak NDVI map changed every year (fig. 5), ranging from late

11

March to early May. While supported by previous research in other mountain ranges (Möhl et al., 2022, 2023; Pirk et al., 2023), our findings contrast with those of Alonso-González et al. (2024), who identified SMOD as the main driver of interannual variability in peak NDVI intensity across the Pyrenees using AVHRR data over a 34-year period. Nonetheless,

240 their use of coarse-resolution imagery (1.1 km) and a much larger study area may obscure fine-scale ecological patterns as those observed in this study in a smaller study area, since lower-resolution satellite products can miss important spatial heterogeneity in vegetation dynamics or report greening trends not observed at ground level (Assmann et al., 2020; Pattison et al., 2015). Our use of Sentinel-2 imagery at 10 m resolution over eight years offers a more detailed view of local-scale processes, but on a shorter span of time, which could limit our ability to observe the effect of SMOD long-term.

245 The meteorological conditions following snowmelt appear to exert a strong influence on peak NDVI intensity (Fig. 4). Previous studies have shown that air temperature and precipitation after melt-out are major controls on alpine grassland growth and biomass (Jonas et al., 2008; Rammig et al., 2010), with June temperature emerging as a key predictor of NDVI variability in some high-latitude regions (Heim et al., 2022). Conversely, summer drought and warming-induced water stress could suppress or reverse greening trends, even when snowmelt was experimentally advanced (Liu et al., 2021; Möhl et al., 2023). Choler et

250 al. (2024) highlighted that late-melting ecosystems are particularly sensitive to climate change because they have experienced the largest proportional increase in heat accumulation during the snow-free period over recent decades. This finding shifts the focus from summer temperature effects toward the cumulative influence of early-season thermal availability—suggesting that extended growing seasons and higher snow-free degree-day sums, rather than warmer summers alone, are increasingly shaping alpine productivity patterns. However, other factors, such as soil parameters regulating water retention and soil nutrition need

255 to be taken into account as additional relevant drivers of peak NDVI intensity (Piedallu et al., 2019).

Given the high spatial stability of the peak NDVI distribution (Fig. 5), we hypothesize that these conditioning factors are intrinsic to the site biophysical properties, rather than an external forcing. While snowmelt patterns present a higher yearly variability, the consistent long-term presence of the snowpack during winter in this environment (Revuelto et al., 2020; Sturm & Wagner, 2010) may have acted as an ecological filter, shaping key soil properties, species composition, and microclimatic

260 conditions that persist across years (Winkler et al., 2018; Wu et al., 2022). This interpretation is supported by recent findings on the legacy of the snow cover on soil ecosystem properties in the Alps (Choler et al., 2025). Myers-Smith et al. (2020) emphasized that NDVI trends can reflect changes in species traits, growth forms, and community composition—factors that are shaped by long-term environmental pressures. Based on this hypothesis, a new perspective emerges for the trend of high NDVI values in intermediate SMOD periods—reported by Revuelto et al. (2022) and also observed in the annual NDVI

265 evolution (Fig. 2) and in the peak NDVI distribution regarding SMOD classification (Fig. 5). We propose that this relationship is not causal but coincidental—areas of high peak NDVI values remain the same throughout the study period because of the underlying physical and biological factors, while meteorological variability drives the timing of SMOD.

From a methodological standpoint, cloud obscuration posed a severe challenge. During our eight-year study, there was a consistent lack of cloud-free images between late May and early June (see the blanks in the NDVI sequence at the top of Fig.

270 4), impeding our analysis during an important stage of growth. The implementation of newly-designed improved cloud and

shadow detection algorithms—such as the one presented by Wright et al. (2025)—could expand usable observations, potentially filling the May-June gaps and improving phenological curve overall accuracy.

These findings have important implications in the current climate change context. While the increasingly shorter Pyrenean snow season (Barrou Dumont et al., 2025; López-Moreno et al., 2017) might theoretically extend the growing season, the

275 actual outcome will depend on precipitation patterns and the ability of alpine communities to adapt to increased drought stress or heat extremes (Möhl et al., 2023). In case of more frequent late spring and summer droughts, as in 2019, productivity can markedly decline. Conversely, years like 2023 show that strong productivity is still possible under earlier melt-out—if moisture and temperature align.

Over longer timescales, changes in snowpack dynamics are likely to reshape vegetation patterns by altering the distribution of

280 site-specific ecological optima (Henn et al., 2024; Spasojevic et al., 2013). Upslope species migration in response to shifting snowmelt regimes may lead to habitat loss for alpine grasslands, particularly due to encroachment by forests and shrublands (Pérez-García et al., 2013). If species are unable to track these upslope shifts quickly enough the resulting mismatch between their climatic requirements and local conditions may lead to declines in productivity and increased community instability (Rogora et al., 2018).

285 ## 6. Conclusions

We analysed the effect of snowmelt timing on grassland dynamics regarding phenology and productivity, with an additional focus on spatial patterns. Additional meteorological data and time-lapse imagery were used to further explore this relationship. While the yearly date of snow disappearance consistently initiates vegetation growth and influences the timing of peak productivity, it does not appear to control its magnitude, which is influenced by post-melt meteorological conditions. The

290 consistency of peak productivity patterns despite higher snowmelt variability indicates an influence of long-term environmental processes instead of a direct link with short-term interannual snowmelt differences.

Our findings and results from previous works highlight the importance of distinguishing between short-term snowmelt fluctuations and the long-term spatial consistency of snow cover in shaping alpine vegetation. Notably, the spatial distribution of peak NDVI remained remarkably stable across years, even as snowmelt timing varied, suggesting that site-specific

295 characteristics exert a stronger influence on productivity than interannual snow dynamics. As climate change continues to alter snowpack duration and melt-out timing, the ecological consequences will depend not only on the timing of snow disappearance but also on the resilience and adaptability of these productive zones. To better understand these dynamics, future research should focus on improving our knowledge about the relative contributions of snowmelt timing across temporal and spatial scales. A multi-platform approach—combining long-term satellite records, UAV-based high-resolution imagery, and in-situ

300 ecological measurements—offers a promising path toward a more mechanistic understanding of how snow dynamics influence alpine productivity, spatial vegetation patterns, and biodiversity under changing climatic regimes.

Data availability

The data supporting the findings of this study are available to reviewers through a private Zenodo link. Upon acceptance of the manuscript, the full dataset will be made publicly accessible in Zenodo and assigned a permanent DOI, which will be

305   provided in the published version of the article.

Author contributions

PDA: Writing – original draft, Visualization, Software, Methodology, Formal analysis. **JR**: Writing – review & editing, Supervision, Funding acquisition, Methodology, Conceptualization. **SG**: Writing – review & editing, Methodology. **JILM**: Writing – review & editing, Supervision, Funding acquisition, Conceptualization.

Competing interests

310

The authors declare that they have no conflict of interest.

Acknowledgements

315

Financial support

References

Alonso-González, E., Ilzarbe-Senosiain, I., Lopez-Moreno, J. I., Lucas-Borja, M. E., Vicente-Serrano, S. M., Beguería, S., & Gascoin, S. (2024). The snow cover is more important than other climatic variables on the prediction of vegetation dynamics
325   in the Pyrenees (1981–2014). *Environmental Research Letters*, *19*(6), 064058. https://doi.org/10.1088/1748-9326/ad4e4c

Alonso-González, E., López-Moreno, J. I., Navarro-Serrano, F., Sanmiguel-Vallelado, A., Revuelto, J., Domínguez-Castro, F., & Ceballos, A. (2020). Snow climatology for the mountains in the Iberian Peninsula using satellite imagery and simulations with dynamically downscaled reanalysis data. *International Journal of Climatology*, *40*(1), 477-491. https://doi.org/10.1002/joc.6223

330   Asam, S., Callegari, M., Matiu, M., Fiore, G., De Gregorio, L., Jacob, A., Menzel, A., Zebisch, M., & Notarnicola, C. (2018). Relationship between Spatiotemporal Variations of Climate, Snow Cover and Plant Phenology over the Alps—An Earth Observation-Based Analysis. *Remote Sensing*, *10*(11), Article 11. https://doi.org/10.3390/rs10111757

Assmann, J. J., Myers-Smith, I. H., Kerby, J. T., Cunliffe, A. M., & Daskalova, G. N. (2020). Drone data reveal heterogeneity in tundra greenness and phenology not captured by satellites. *Environmental Research Letters*, *15*(12), 125002.

335   https://doi.org/10.1088/1748-9326/abbf7d

Baptist, F., Flahaut, C., Streb, P., & Choler, P. (2010). No increase in alpine snowbed productivity in response to experimental lengthening of the growing season. *Plant Biology*, *12*(5), 755-764. https://doi.org/10.1111/j.1438-8677.2009.00286.x

Barrou Dumont, Z., Gascoin, S., Inglada, J., Dietz, A., Köhler, J., Lafaysse, M., Monteiro, D., Carmagnola, C., Bayle, A., Dedieu, J.-P., Hagolle, O., & Choler, P. (2025). Trends in the annual snow melt-out day over the French Alps and Pyrenees

340   from 38 years of high-resolution satellite data (1986–2023). *The Cryosphere*, *19*(7), 2407-2429. https://doi.org/10.5194/tc-19-2407-2025

Bayle, A., Gascoin, S., Corona, C., Stoffel, M., & Choler, P. (2025). Snow melt-out date (SMOD) change spanning four decades in European temperate mountains at 30 m from Landsat time series. *Scientific Data*, *12*(1), 706. https://doi.org/10.1038/s41597-025-05044-2

345   Beniston, M., Farinotti, D., Stoffel, M., Andreassen, L. M., Coppola, E., Eckert, N., Fantini, A., Giacona, F., Hauck, C., Huss, M., Huwald, H., Lehning, M., López-Moreno, J.-I., Magnusson, J., Marty, C., Morán-Tejéda, E., Morin, S., Naaim, M., Provenzale, A., … Vincent, C. (2018). The European mountain cryosphere: A review of its current state, trends, and future challenges. *The Cryosphere*, *12*(2), 759-794. https://doi.org/10.5194/tc-12-759-2018

Chen, R., Yin, G., Liu, G., Li, J., & Verger, A. (2020). Evaluation and Normalization of Topographic Effects on Vegetation

350   Indices. *Remote Sensing*, *12*(14), Article 14. https://doi.org/10.3390/rs12142290

Choler, P. (2015). Growth response of temperate mountain grasslands to inter-annual variations in snow cover duration. *Biogeosciences*, *12*(12), 3885-3897. https://doi.org/10.5194/bg-12-3885-2015

Choler, P., Bayle, A., Fort, N., & Gascoin, S. (2024). Waning snowfields have transformed into hotspots of greening within the alpine zone. *Nature Climate Change*, 1-6. https://doi.org/10.1038/s41558-024-02177-x

355   Choler, P., Bonfanti, N., Reverdy, A., Bayle, A., Nicoud, B., Liger, L., Clément, J.-C., Cohard, J.-M., Corona, C., Gascoin, S., Voisin, D., & Poulenard, J. (2025). Legacy of snow cover on alpine landscapes. *Communications Earth & Environment*, *6*(1), 758. https://doi.org/10.1038/s43247-025-02702-6

Copernicus Climate Change Service (C3S). (2024). *European State of the Climate 2023 | Copernicus*. https://doi.org/10.24381/BS9V-8C66

15

360   Dedieu, J.-P., Carlson, B. Z., Bigot, S., Sirguey, P., Vionnet, V., & Choler, P. (2016). On the Importance of High-Resolution Time Series of Optical Imagery for Quantifying the Effects of Snow Cover Duration on Alpine Plant Habitat. *Remote Sensing*, *8*(6), Article 6. https://doi.org/10.3390/rs8060481

Dong, D., Wang, C., Yan, J., He, Q., Zeng, J., & Wei, Z. (2020). Combing Sentinel-1 and Sentinel-2 image time series for invasive Spartina alterniflora mapping on Google Earth Engine: A case study in Zhangjiang Estuary. *Journal of Applied*

365   *Remote Sensing*, *14*(4), 044504. https://doi.org/10.1117/1.JRS.14.044504

Du, Y., Zhang, Y., Ling, F., Wang, Q., Li, W., & Li, X. (2016). Water Bodies' Mapping from Sentinel-2 Imagery with Modified Normalized Difference Water Index at 10-m Spatial Resolution Produced by Sharpening the SWIR Band. *Remote Sensing*, *8*(4), 354. https://doi.org/10.3390/rs8040354

Dumont, M., Monteiro, D., Filhol, S., Gascoin, S., Marty, C., Hagenmuller, P., Morin, S., Choler, P., & Thuiller, W. (2025).

370   The European Alps in a changing climate: Physical trends and impacts. *Comptes Rendus. Géoscience*, *357*(G1), 25-42. https://doi.org/10.5802/crgeos.288

Fontana, F., Rixen, C., Jonas, T., Aberegg, G., & Wunderle, S. (2008). Alpine Grassland Phenology as Seen in AVHRR, VEGETATION, and MODIS NDVI Time Series—A Comparison with In Situ Measurements. *Sensors*, *8*(4), Article 4. https://doi.org/10.3390/s8042833

375   Gao, X., Chi, H., Huang, J., Han, Y., Li, Y., & Ling, F. (2024). Comparison of Cloud-Mask Algorithms and Machine-Learning Methods Using Sentinel-2 Imagery for Mapping Paddy Rice in Jianghan Plain. *Remote Sensing*, *16*(7), Article 7. https://doi.org/10.3390/rs16071305

Gascoin, S., Grizonnet, M., Bouchet, M., Salgues, G., & Hagolle, O. (2019). *Theia Snow collection: High-resolution operational snow cover maps from Sentinel-2 and Landsat-8 data*.

380   Hall, D. K., Riggs, G. A., & Salomonson, V. V. (1995). Development of methods for mapping global snow cover using moderate resolution imaging spectroradiometer data. *Remote Sensing of Environment*, *54*(2), 127-140. https://doi.org/10.1016/0034-4257(95)00137-P

Heim, B., Lisovski, S., Wieczorek, M., Morgenstern, A., Juhls, B., Shevtsova, I., Kruse, S., Boike, J., Fedorova, I., & Herzschuh, U. (2022). Spring snow cover duration and tundra greenness in the Lena Delta, Siberia: Two decades of MODIS

385   satellite time series (2001–2021). *Environmental Research Letters*, *17*(8), 085005. https://doi.org/10.1088/1748-9326/ac8066

Henn, J. J., Anderson, K. E., Brigham, L. M., Bueno de Mesquita, C. P., Collins, C. G., Elmendorf, S. C., Green, M. D., Huxley, J. D., Rafferty, N. E., Rose-Person, A., & Spasojevic, M. J. (2024). Long-Term Alpine Plant Responses to Global Change Drivers Depend on Functional Traits. *Ecology Letters*, *27*(10), e14518. https://doi.org/10.1111/ele.14518

Jonas, T., Rixen, C., Sturm, M., & Stoeckli, V. (2008). How alpine plant growth is linked to snow cover and climate variability.

390   *Journal of Geophysical Research: Biogeosciences*, *113*(G3). https://doi.org/10.1029/2007JG000680

Körner, C. (2021). *Alpine Plant Life: Functional Plant Ecology of High Mountain Ecosystems*. Springer International Publishing. https://doi.org/10.1007/978-3-030-59538-8

Kotlarski, S., Gobiet, A., Morin, S., Olefs, M., Rajczak, J., & Samacoïts, R. (2023). 21st Century alpine climate change. *Climate Dynamics*, *60*(1-2), 65-86. https://doi.org/10.1007/s00382-022-06303-3

395 Liu, Y., Li, Z., & Chen, Y. (2021). Continuous warming shift greening towards browning in the Southeast and Northwest High Mountain Asia. *Scientific Reports*, *11*(1), 17920. https://doi.org/10.1038/s41598-021-97240-4

López-Moreno, J. I., Gascoin, S., Herrero, J., Sproles, E. A., Pons, M., Alonso-González, E., Hanich, L., Boudhar, A., Musselman, K. N., Molotch, N. P., Sickman, J., & Pomeroy, J. (2017). Different sensitivities of snowpacks to warming in Mediterranean climate mountain areas. *Environmental Research Letters*, *12*(7), 074006. https://doi.org/10.1088/1748-400 9326/aa70cb

López-Moreno, J. I., Soubeyroux, J. M., Gascoin, S., Alonso-Gonzalez, E., Durán-Gómez, N., Lafaysse, M., Vernay, M., Carmagnola, C., & Morin, S. (2020). Long-term trends (1958–2017) in snow cover duration and depth in the Pyrenees. *International Journal of Climatology*, *40*(14), 6122-6136. https://doi.org/10.1002/joc.6571

Mascetti, G., Gentili, R., Ferré, C., Fuccella, R., Agaba, S., Pricca, N., Cabassi, G., Povolo, M., & Comolli, R. (2023).
405 Sustainable management, critical issues and environmental services of a pastoral system in the Central Alps. *Biodiversity*, *24*(1-2), 79-84. https://doi.org/10.1080/14888386.2023.2192687

Möhl, P., von Büren, R. S., & Hiltbrunner, E. (2022). Growth of alpine grassland will start and stop earlier under climate warming. *Nature Communications*, *13*(1), 7398. https://doi.org/10.1038/s41467-022-35194-5

Möhl, P., Vorkauf, M., Kahmen, A., & Hiltbrunner, E. (2023). Recurrent summer drought affects biomass production and
410 community composition independently of snowmelt manipulation in alpine grassland. *Journal of Ecology*, *111*(11), 2357-2375. https://doi.org/10.1111/1365-2745.14180

Mullerova, D., & Williams, M. (2019). Satellite Monitoring of Thermal Performance in Smart Urban Designs. *Remote Sensing*, *11*(19), Article 19. https://doi.org/10.3390/rs11192244

Myers-Smith, I. H., Kerby, J. T., Phoenix, G. K., Bjerke, J. W., Epstein, H. E., Assmann, J. J., John, C., Andreu-Hayles, L.,
415 Angers-Blondin, S., Beck, P. S. A., Berner, L. T., Bhatt, U. S., Bjorkman, A. D., Blok, D., Bryn, A., Christiansen, C. T., Cornelissen, J. H. C., Cunliffe, A. M., Elmendorf, S. C., … Wipf, S. (2020). Complexity revealed in the greening of the Arctic. *Nature Climate Change*, *10*(2), 106-117. https://doi.org/10.1038/s41558-019-0688-1

Mzid, N., Pignatti, S., Huang, W., & Casa, R. (2021). An Analysis of Bare Soil Occurrence in Arable Croplands for Remote Sensing Topsoil Applications. *Remote Sensing*, *13*(3), 474. https://doi.org/10.3390/rs13030474

420 Pattison, R. R., Jorgenson, J. C., Raynolds, M. K., & Welker, J. M. (2015). Trends in NDVI and Tundra Community Composition in the Arctic of NE Alaska Between 1984 and 2009. *Ecosystems*, *18*(4), 707-719. https://doi.org/10.1007/s10021-015-9858-9

Pérez-García, N., Font, X., Ferré, A., & Carreras, J. (2013). Drastic reduction in the potential habitats for alpine and subalpine vegetation in the Pyrenees due to twenty-first-century climate change. *Regional Environmental Change*, *13*(6), 1157-1169.
425 https://doi.org/10.1007/s10113-013-0427-5

Piedallu, C., Chéret, V., Denux, J. P., Perez, V., Azcona, J. S., Seynave, I., & Gégout, J. C. (2019). Soil and climate differently impact NDVI patterns according to the season and the stand type. *Science of The Total Environment*, *651*, 2874-2885. https://doi.org/10.1016/j.scitotenv.2018.10.052

Pirk, N., Aalstad, K., Yilmaz, Y. A., Vatne, A., Popp, A. L., Horvath, P., Bryn, A., Vollsnes, A. V., Westermann, S., Berntsen,
430 T. K., Stordal, F., & Tallaksen, L. M. (2023). Snow–vegetation–atmosphere interactions in alpine tundra. *Biogeosciences*, *20*(11), 2031-2047. https://doi.org/10.5194/bg-20-2031-2023

Qian, D., Fan, B., Lan, Y., Si, M., Li, Q., & Guo, X. (2023). Ecosystem Service Relationships, Drivers, and Regulation Strategies in a Degraded Alpine Shrub Meadow on the Northeastern Qinghai-Tibetan Plateau. *Diversity*, *15*(5), Article 5. https://doi.org/10.3390/d15050596

435 Rammig, A., Jonas, T., Zimmermann, N. E., & Rixen, C. (2010). Changes in alpine plant growth under future climate conditions. *Biogeosciences*, *7*(6), 2013-2024. https://doi.org/10.5194/bg-7-2013-2010

Revuelto, J., Alonso-González, E., & López-Moreno, J. I. (2020). Generation of daily high-spatial resolution snow depth maps from in-situ measurement and time-lapse photographs. *Cuadernos de Investigación Geográfica*, *46*(1), 59-79. https://doi.org/10.18172/cig.3801

440 Revuelto, J., Azorin-Molina, C., Alonso-González, E., Sanmiguel-Vallelado, A., Navarro-Serrano, F., Rico, I., & López-Moreno, J. I. (2017). Meteorological and snow distribution data in the Izas Experimental Catchment (Spanish Pyrenees) from 2011 to 2017. *Earth System Science Data*, *9*(2), 993-1005. https://doi.org/10.5194/essd-9-993-2017

Revuelto, J., Gómez, D., Alonso-González, E., Vidaller, I., Rojas-Heredia, F., Deschamps-Berger, C., García-Jiménez, J., Rodríguez-López, G., Sobrino, J., Montorio, R., Perez-Cabello, F., & López-Moreno, J. I. (2022). Intermediate snowpack
445 melt-out dates guarantee the highest seasonal grasslands greening in the Pyrenees. *Scientific Reports*, *12*(1), 18328. https://doi.org/10.1038/s41598-022-22391-x

Revuelto, J., Jonas, T., & López-Moreno, J.-I. (2016). Backward snow depth reconstruction at high spatial resolution based on time-lapse photography. *Hydrological Processes*, *30*(17), 2976-2990. https://doi.org/10.1002/hyp.10823

Revuelto, J., López-Moreno, J. I., Azorin-Molina, C., & Vicente-Serrano, S. M. (2014). Topographic control of snowpack
450 distribution in a small catchment in the central Spanish Pyrenees: Intra- and inter-annual persistence. *The Cryosphere*, *8*(5), 1989-2006. https://doi.org/10.5194/tc-8-1989-2014

Riihimäki, H., Heiskanen, J., & Luoto, M. (2017). The effect of topography on arctic-alpine aboveground biomass and NDVI patterns. *International Journal of Applied Earth Observation and Geoinformation*, *56*, 44-53. https://doi.org/10.1016/j.jag.2016.11.005

455 Rogora, M., Frate, L., Carranza, M. L., Freppaz, M., Stanisci, A., Bertani, I., Bottarin, R., Brambilla, A., Canullo, R., Carbognani, M., Cerrato, C., Chelli, S., Cremonese, E., Cutini, M., Musciano, M. D., Erschbamer, B., Godone, D., Iocchi, M., Isabellon, M., … Matteucci, G. (2018). Assessment of climate change effects on mountain ecosystems through a cross-site analysis in the Alps and Apennines. *Science of The Total Environment*, *624*, 1429-1442. https://doi.org/10.1016/j.scitotenv.2017.12.155

460   Skakun, S., Wevers, J., Brockmann, C., Doxani, G., Aleksandrov, M., Batič, M., Frantz, D., Gascon, F., Gómez-Chova, L., Hagolle, O., López-Puigdollers, D., Louis, J., Lubej, M., Mateo-García, G., Osman, J., Peressutti, D., Pflug, B., Puc, J., Richter, R., … Žust, L. (2022). Cloud Mask Intercomparison eXercise (CMIX): An evaluation of cloud masking algorithms for Landsat 8 and Sentinel-2. *Remote Sensing of Environment*, *274*, 112990. https://doi.org/10.1016/j.rse.2022.112990

Slatyer, R. A., Umbers, K. D. L., & Arnold, P. A. (2022). Ecological responses to variation in seasonal snow cover.
465   *Conservation Biology*, *36*(1), e13727. https://doi.org/10.1111/cobi.13727

Spasojevic, M. J., Bowman, W. D., Humphries, H. C., Seastedt, T. R., & Suding, K. N. (2013). Changes in alpine vegetation over 21 years: Are patterns across a heterogeneous landscape consistent with predictions? *Ecosphere*, *4*(9), art117. https://doi.org/10.1890/ES13-00133.1

Sturm, M., & Wagner, A. M. (2010). Using repeated patterns in snow distribution modeling: An Arctic example. *Water*
470   *Resources Research*, *46*(12). https://doi.org/10.1029/2010WR009434

Tomaszewska, M. A., Nguyen, L. H., & Henebry, G. M. (2020). Land surface phenology in the highland pastures of montane Central Asia: Interactions with snow cover seasonality and terrain characteristics. *Remote Sensing of Environment*, *240*, 111675. https://doi.org/10.1016/j.rse.2020.111675

Vitasse, Y., Rebetez, M., Filippa, G., Cremonese, E., Klein, G., & Rixen, C. (2017). 'Hearing' alpine plants growing after
475   snowmelt: Ultrasonic snow sensors provide long-term series of alpine plant phenology. *International Journal of Biometeorology*, *61*(2), 349-361. https://doi.org/10.1007/s00484-016-1216-x

Vorkauf, M., Kahmen, A., Körner, C., & Hiltbrunner, E. (2021). Flowering phenology in alpine grassland strongly responds to shifts in snowmelt but weakly to summer drought. *Alpine Botany*, *131*(1), 73-88. https://doi.org/10.1007/s00035-021-00252-z

480   Vorkauf, M., Marty, C., Kahmen, A., & Hiltbrunner, E. (2021). Past and future snowmelt trends in the Swiss Alps: The role of temperature and snowpack. *Climatic Change*, *165*(3), 44. https://doi.org/10.1007/s10584-021-03027-x

Winkler, D. E., Butz, R. J., Germino, M. J., Reinhardt, K., & Kueppers, L. M. (2018). Snowmelt Timing Regulates Community Composition, Phenology, and Physiological Performance of Alpine Plants. *Frontiers in Plant Science*, *9*. https://doi.org/10.3389/fpls.2018.01140

485   Wright, N., Duncan, J. M. A., Callow, J. N., Thompson, S. E., & George, R. J. (2025). Training sensor-agnostic deep learning models for remote sensing: Achieving state-of-the-art cloud and cloud shadow identification with OmniCloudMask. *Remote Sensing of Environment*, *322*, 114694. https://doi.org/10.1016/j.rse.2025.114694

Wu, M., Liu, Z., Chen, L., Pang, D., Xu, X., Zhang, Y., Ni, X., Hu, Y., & Li, X. (2022). Elevation gradient shapes microbial carbon and phosphorous limitations in the Helan Mountains, Northwest China. *Frontiers in Environmental Science*, *10*.
490   https://doi.org/10.3389/fenvs.2022.1041964

Xie, J., Jonas, T., Rixen, C., de Jong, R., Garonna, I., Notarnicola, C., Asam, S., Schaepman, M. E., & Kneubühler, M. (2020). Land surface phenology and greenness in Alpine grasslands driven by seasonal snow and meteorological factors. *Science of The Total Environment*, *725*, 138380. https://doi.org/10.1016/j.scitotenv.2020.138380

Zupanc, A., 2017. Improving Cloud Detection with Machine Learning. https://medium. com/sentinel-hub/improving-cloud-
495   detection-with-machine-learning-c09dc5d7cf13 (accessed 13 June 2025)